Current Research in Neurobiology 5 (2023) 100105

Contents lists available at ScienceDirect

Current Research in Neurobiology

journal homepage: www.sciencedirect.com/journal/current-research-in-neurobiology

Propranolol reduces the accumulation of cytotoxic aggregates in C9orf72-ALS/FTD *in vitro* models

Mira Seidel [a,1], Sandeep Rajkumar [a,1], Christina Steffke [a], Vivien Noeth [a,b], Shreya Agarwal [a,b], Kevin Roger [c], Joanna Lipecka [c], Albert Ludolph [d,e], Chiara Ida Guerrera [c], Tobias Boeckers [a,e], Alberto Catanese [a,e,*]

[a] Institute of Anatomy and Cell Biology, Ulm University School of Medicine, Ulm, Germany
[b] International Graduate School in Molecular Medicine, Ulm University, Ulm, Germany
[c] Proteomics Platform Necker, Université Paris Cité - Structure Fédérative de Recherche Necker, INSERM US24/CNRS UAR3633, Paris, France
[d] Department of Neurology, Ulm University School of Medicine, Ulm, Germany
[e] Deutsches Zentrum für Neurodegenerative Erkrankungen (DZNE), Ulm site, Ulm, Germany

ARTICLE INFO

Keywords:
ALS
FTD
Aggregates
Poly(GA)
Autophagy
Lysosomes
C9orf72
hiPSC
Neurodegeneration
Neurons

ABSTRACT

Mutations in the *C9orf72* gene are the most common cause of familial amyotrophic lateral sclerosis (ALS) and frontotemporal dementia (FTD). The pathogenetic mechanisms linked to this gene are a direct consequence of an aberrant intronic expansion of a GGGGCC hexanucleotide located between the 1a and 1b non-coding exons, which can be transcribed to form cytotoxic RNA foci or even translated into aggregation-prone dipeptide repeat proteins. Importantly, the abnormal length of these repeats affects also the expression levels of C9orf72 itself, which suggests haploinsufficiency as additional pathomechanism. Thus, it appears that both toxic gain of function and loss of function are distinct but still coexistent features contributing to the insurgence of the disease in case of C9orf72 mutations. In this study, we aimed at identifying a strategy to address both aspects of the C9orf72-related pathobiochemistry and provide proof-of-principle information for a better understanding of the mechanisms leading to neuronal loss. By using primary neurons overexpressing toxic poly(GA), the most abundant protein product of the GGGGCC repeats, we found that the antiarrhythmic drug propranolol could efficiently reduce the accumulation of aberrant aggregates and increase the survival of C9orf72-related cultures. Interestingly, the improved catabolism appeared to not depend on major degradative pathways such as autophagy and the proteasome. By analyzing the proteome of poly(GA)-expressing neurons after exposure to propranolol, we found that the drug increased lysosomal degradation through a mechanism directly involving C9orf72 protein, whose levels were increased after treatment. Further confirmation of the beneficial effect of the beta blocker on aggregates' accumulation and survival of hiPSC-derived C9orf72-mutant motoneurons strengthened the finding that addressing both facets of C9orf72 pathology might represent a valid strategy for the treatment of these ALS/FTD cases.

1. Introduction

The accumulation of toxic protein aggregates is a pathological feature characterizing several neurodegenerative conditions, such as aberrant extracellular beta amyloid plaques and intracellular hyperphosphorylated tau inclusions in Alzheimer's disease (AD), mutant huntingtin aggregates in Huntington's disease, and Lewy bodies in Parkinson's disease (PD) (reviewed by Ross and Poirier, 2004). Along the same line, aberrant aggregates are also detected within the motor neurons of patients suffering from amyotrophic lateral sclerosis (ALS). Importantly, an intronic hexanucleotide-repeat expansion (HRE) in the C9orf72 gene has been identified as the most common genetic cause of both ALS and frontotemporal dementia (FTD) (DeJesus-Hernandez et al., 2011; Burrell et al., 2016). This HRE is translated in an AUG-independent manner from both sense and antisense transcripts in all reading frames into five dipeptide repeat proteins (DPRs): poly(GA),

* Corresponding author. Institute of Anatomy and Cell Biology, Ulm University School of Medicine, Ulm, Germany.
E-mail address: alberto.catanese@uni-ulm.de (A. Catanese).
[1] Co-first authors.

https://doi.org/10.1016/j.crneur.2023.100105
Received 25 January 2023; Received in revised form 23 June 2023; Accepted 26 July 2023
Available online 30 July 2023

poly(GR), poly(GP), poly(PR) and poly(PA) (Mori et al., 2013; Zu et al., 2013). In *post-mortem* samples from C9orf72 patient brains, poly(GA) constitutes the majority of TDP-43-negative inclusions, which can be attributed to its highly aggregation-prone, amyloid-like (biophysical) properties (Chang et al., 2016; Edbauer and Haass, 2016; Brasseur et al., 2020). Its toxic characteristics have been suggested to result in the sequestration of other molecules such as SQSTM1/p62 and Unc119, which play a crucial role in catabolic processes (Maduro et al., 2000; May et al., 2014), as well as proteasomal subunits (Zhang et al., 2014; Khosravi et al., 2020). This leads to a disruption of protein degradation systems and, eventually, neuronal loss (May et al., 2014; Zhang et al., 2014; Khosravi et al., 2020; Catanese et al., 2021). In addition, the CCCCGG-transcripts form nuclear RNA-foci that sequestrate and subsequently disable some major ribonucleic-binding proteins (RBP), thus linking altered RNA metabolism to the C9orf72 pathobiochemistry (DeJesus-Hernandez et al., 2011). As a third pathomechanism, it has been shown that HRE reduces the expression of C9orf72 transcripts, and the resulting haploinsufficiency seems to depend on epigenetic alterations (Xi et al., 2013; Belzil et al., 2013; Gijselinck et al., 2016). Interestingly, loss of C9orf72 has been shown to alter neuronal morphology and impair autophagy initiation, as well as the endolysosomal pathway (Levine et al., 2013; Farg et al., 2014; Sullivanet al., 2016; Sellier et al., 2016; Ho et al., 2019). Thus, the loss of C9orf72 might impact key catabolic mechanisms, resulting in an inefficient degradation of toxic aggregates that further exacerbates the HRE toxic gain of function in a pathologic vicious circle leading to neuronal death. Interestingly, catabolic impairments are not exclusively observed in the presence of C9orf72 mutations, but represent a commonly shared pathomechanism among heterogenous cases of ALS/FTD. In fact, mutations in several other genes associated with autophagy and/or lysosomal function such *GRN*, *VCP*, *CHMP2B*, *SQSTM1*, *OPTN* and *TBK1* have been causally linked to FTD and ALS.

While these observations suggest that autophagy modulation might represent a promising therapeutic strategy to reduce the aggregates' burden and relieve vulnerable neurons from high levels of cellular stress, the evidences in support of this theory have been inconsistent. Though some recent studies have demonstrated that increased autophagy efficiently clears intracellular aggregates (Cheng et al., 2015; Boivin et al., 2020), contrasting results have demonstrated that autophagy induction exacerbates the burden of protein aggregates in vulnerable neurons and contributes in speeding up the disease progression by creating an autophagy overload (Zhang et al., 2011; Saxena et al., 2013; Catanese et al., 2019). Indeed, autophagy blockade through ATG7 knockout significantly increases the lifespan of the SOD1-G93A mutant mice (Rudnick et al., 2017).

Interestingly, a recent retrospective study linked the use of beta-blockers with high blood-brain barrier permeability, such as propranolol, to a decreased risk of developing AD (Beaman et al., 2023). Given the lysosomotropic properties of this beta blocker (Müller et al., 2020) and the still controversial role of autophagy induction in ALS/FTD, in the present work we aimed at better characterizing the consequences of toxic aggregates accumulation in ALS/FTD C9orf72-related models and to test the potential beneficial effect of propranolol in the clearance of these pathologic structures from affected neurons.

2. Materials and methods

2.1. Primary rat cortical neurons

Primary cultures of rat cortical neurons were prepared from rat embryos (Sprague-Dawley rats, Janvier Laboratories) at embryonic day 18 as described previously (Catanese et al., 2018). Briefly, cerebral cortices were manually dissected under stereomicroscopic guidance. After 10 min of incubation with 0.25% trypsin-EDTA (Gibco), the tissues were washed three times with DMEM (Gibco) (containing 10% foetal bovine serum, 1% penicillin/streptomycin, and 1% GlutaMAX, henceforth referred to as DMEM+) and thus mechanically dissociated. Following a filtration through a 100 μm mesh filter, the dissociated cells were plated on poly-L-lysine-coated (Sigma-Aldrich) glass coverslips or plastic dishes and cultured in Neurobasal Medium (Gibco) (containing 1% P/S, 1% GlutaMAX and 2% B27 – henceforth NB^+).

The expression of poly-$(GA)_{175}$-EGFP aggregates in primary neurons was performed using an AAV9 vector; expression of the ALS construct was under the control of the human Synapsin 1 promoter to ensure selective neuronal expression. Viruses were produced by the Penn Vector Core (University of Pennsylvania, Philadelphia, USA). Transduction of neurons was performed at DIV 3 with either AAV9-hSyn-poly$(GA)_{175}$-EGFP or AAV9-hSyn-EGFP (a gift from Bryan Roth; Addgene viral prep # 50 465-AAV9).

2.2. Pharmacological treatment

Primary and hiPSC-derived neurons were treated with (S)-(-)-Propranolol (Sigma-Aldrich, P8688) at a 10 μM concentration for 24 h, except when we evaluated the effect of the beta blocker on neuronal survival: in this case neuronal cultures were treated for 72 h by replacing half of the medium on the second and third day of treatment.

For the investigation of the autophagic flux, we used bafilomycin (Sigma-Aldrich, B1793) at a concentration of 100 nM. The lysosome blocker E-64 (Tocris, 4545) was used at a final concentration of 10 μM.

2.3. Immunocytochemistry

Immunostainings were performed as previously described (Catanese et al., 2021). Following fixation with 4% paraformaldehyde (containing 10% sucrose), cells were first incubated with blocking solution (PBS + 10% Goat Serum + 0.2% Triton-x100) for 2 h and subsequently with primary antibodies diluted in the same blocking solution overnight (24 h at 4 °C). After three washes with PBS, the cells were incubated with secondary antibodies (diluted 1:1000 in PBS) for 2 h at room temperature. Then, cells were washed again 3 times and mounted with ProLong™ Gold Antifade mountant with DAPI (Invitrogen, P36935) and ibidi Mounting Medium (Ibidi, 5001).

2.4. Microscopy

Fluorescence microscopy was performed with a Thunder imaging system (Leica) equipped with a DFC9000 sCMOS camera, a HC PL Fluotar 20x air (N.A. 0.4) or a HC PL Apo 63x (N.A. 1.4) oil immersion objective and using the LasX software (Leica).

Confocal microscopy was performed with a laser-scanning microscope (Leica DMi8) equipped with ACS APO 40x and 63x oil DIC immersion objectives. Images were acquired using the LasX software (Leica), with a resolution of 1024x1024 pixels and a number of Z-stacks (step size of 0.3 or 0.5 μm) encompassing the entire cell soma.

2.5. Image analysis

To analyze the number of cleaved caspase-3+ neurons, the signal of the apoptotic markers was thresholded and overlapped to the MAP2 channel. Afterwards, the number of cleaved caspase-3-MAP2 double-positive cells was manually counted.

The number of LAMP1 structures was assessed by using the plug-in Find Foci for Fiji after having defined a region of interest (ROI) around the neuronal soma.

The load of poly(GA) aggregates within the cell body of the primary neurons transduced with poly-$(GA)_{175}$-EGFP, the respective channel was thresholded to distinguish GFP-positive aggregates and the area taken up by these was set into relation with the total soma area to reflect the percentage of cytosol occupied by these aberrant structures. The same procedure was also applied for the analysis of SQSTM1/p62 aggregates.

The colocalization analysis was performed with the semi-automated

colocalization tool of the IMARIS software (Oxford Instrument).

To analyze the cluster size and intensity of synaptic markers, 3 different primary dendrites for each neuron were randomly selected. A ROI was then drawn along the dendrites and synaptic clusters traced with the ImageJ plugin FindFoci (Herbert), using the Max Entropy algorithm and the resulting data was normalized to a ROI length of 10 μm.

The computational parameters and post-acquisition modifications were equally applied to analyze pictures belonging to the same experiments and for figure display, which was performed with either Fiji or Imaris.

2.6. Western blot

Western blots were performed by resolving equal concentrations of protein (determined by Bradford Assay) on 10% acrylamide SDS-PAGE gels, which were then transferred to a nitrocellulose membrane using a Trans-Blot Turbo device (BioRad, USA). To block non-specific binding sites, the membranes were incubated with a 5% BSA solution (diluted in TBS pH 7.5 + 0.2% TWEEN) for 2 h and incubated with the primary antibody overnight at 4 °C. Afterwards, blots were washed 3 times with TBS+0.2% TWEEN, incubated with HRP-conjugated secondary Ab (DAKO) for 1 h, and again washed. Chemiluminescent signal was detected using ECL detection kit (ThermoFischer Scientific, 32 106) and a MicroChemi 4.2 device (DNR Bio Imaging System). For quantification, Gel-analyzer Software 2010a was used. The values of the proteins of interest were normalized against the loading control β-actin.

2.7. Antibody list

In this study, the following primary antibodies were used: anti-MAP2 (Encor, CPCA-MAP2), anti-LC3A (Cell Signaling, 4599), anti-ChAT (custom made by Abcam in rat using the same epitope as ab181023), anti-Synaptophysin (Abcam, ab14692), Homer1 b/c (Synaptic Systems, 160 025), anti-LAMP1 (Invitrogen, MA1-164), anti-cleaved caspase 3 (Cell Signaling, 9661), anti-ubiquitin (Abcam, ab7254), anti-C9orf72 (Genetex, GTX632041, anti-β-actin (Sigma-Aldrich, A5441), anti-RagC (Cell Signaling, 9480), anti-FLCN (Proteintech, 11236-2-AP), anti-NPRL2 (Cell Signaling, 37 344).

For western blot experiments, we used HRP-conjugated anti-Mouse purchased from DAKO.

For immunostainings, the following secondary antibodies from ThermoFisher Scientific were used: goat anti-Chicken DyLight 350 (SA5-10069), goat anti-Mouse Alexa Fluor® 488 (A-11001), goat anti-Rabbit Alexa Fluor® 488 (A-11008), goat anti-Mouse Alexa Fluor® 568 (A-11004), goat anti-Rabbit Alexa Fluor® 568 (A-11011), goat anti-Chicken Alexa Fluor® 647 (A32933), goat anti-Mouse Alexa Fluor® 647 (A-21235), goat anti-Rabbit Alexa Fluor® 647 (A-21244).

2.8. Proteasome activity assay

Proteasomal Activity under treatment conditions was examined by using a Proteasome Activity Assay Kit (Abcam, ab107921). The Assay was performed according to the protocol provided by the manufacturer. Briefly, lysates were prepared using 0.5% NP-40 (Thermo Fisher, 85 124) in PBS (-/-) and added to an opaque 96-well plate and filled up to 100 μl with Assay Buffer. Next, either 1 μl of Assay Buffer or Proteasome inhibitor was added to each sample well to discern non-proteasome activity. Finally, 1 μl of Proteasome Substrate was added to all wells and incubated at 37 °C. Proteolytic activity was measured as fluorescent signal at Ex/Em 350/440 nM in a Gen5 microplate reader (BioTek) at T1 (20 min) and T2 (40 min). To calculate the proteasomal activity the non-proteasome activity was substracted from the total proteolytic activity at both time points (T1 & T2) and the activity at T1 is substracted from the activity a T2 to quantify the proteasome substrate turnover over time.

2.9. qRT-PCR

The RNeasy Mini kit (Qiagen) was used following the protocol provided by the manufacturer for mRNA extraction. First strand synthesis and quantitative real-time-PCR amplification were performed in a one-step, single-tube format using the QuantiFast™ SYBR Green RT-PCR kit from Qiagen according to the manufacturer's instructions in a total volume of 20 μl. The primers used for qRT-PCR were purchased (Qiagen QuantiTect Primer Assays, Qiagen - validated primers without sequence information). The following settings were used: 10 min at 55 °C and 5 min at 95 °C, followed by 40 cycles of PCR for 5 s at 95 °C for denaturation and 10 s at 60 °C for annealing and elongation (one-step). The SYBR Green I reporter dye signal was measured against the internal passive reference dye (ROX) to normalize non-PCR-related fluctuations. The Rotor-Gene Q software (version 2.0.2) was used to calculate the cycle threshold values.

2.10. Mass-spectrometry

S-TrapTM micro spin column (Protifi, Hutington, USA) digestion was performed on 50 μg of primary rat neurons lysates according to manufacturer's instructions. Briefly, samples were supplemented with 20% SDS to a final concentration of 5%, reduced with 20 mM TCEP (Tris(2-carboxyethyl) phosphine hydrochloride) and alkylated with 50 mM CAA (chloracetamide) for 5min at 95 °C. Aqueous phosphoric acid was then added to a final concentration of 2.5% following by the addition of S-Trap binding buffer (90% aqueous methanol, 100 mM TEAB, pH7.1). Mixtures were then loaded on S-Trap columns. Five washes were performed for thorough SDS elimination. Samples were digested with 2.5 μg of trypsin (Promega) at 47 °C for 2h. After elution, peptides were vacuum dried and resuspended in 2% ACN, 0.1% formic acid in HPLC-grade water prior to MS analysis.

The tryptic peptides were resuspended in 250 μL and 400 ng were injected on a nanoelute (Bruker Daltonics, Germany) HPLC (high-performance liquid chromatography) system coupled to a timsTOF Pro (Bruker Daltonics, Germany) mass spectrometer. HPLC separation (Solvent A: 0.1% formic acid in water, 2% acetonitrile; Solvent B: 0.1% formic acid in acetonitrile) was carried out at 250 nL/min using a packed emitter column (C18, 25 cm × 75 μm 1.6 μm) (Ion Optics, Australia) using a 70min gradient elution (2 to 13% solvent B during 42min; 13 to 20% during 23min; 20% to 30% during 5min; 30% to 85% for 5min and finally 80% for 5min to wash the column). Mass-spectrometric data were acquired using the parallel accumulation serial fragmentation (PASEF) acquisition method in DIA mode. The measurements were carried out over the m/z range from 100 to 1700 Th. The range of ion mobilities values from 0.6 to 1.6 V s/cm2(1/k0). The total cycle time was set to 1.5s and the number of PASEF MS/MS scans was set to 10.

2.11. Human iPSCs

In this study, 3 hiPSC lines from ALS patients with C9orf72 HRE have been used: the line $ALS^{C9orf72}$ I was reprogrammed at the Ulm University (Catanese et al., 2019), while the other two were commercially purchased from the Stem Cell Core of Cedars-Sinai (Los Angeles, USA): $ALS^{C9orf72}$ II (CS29iALS-C9nxx) and $ALS^{C9orf72}$ III Cedars-Sinai (CS30iALS-C9nxx). All these lines have been previously characterized (Catanese et al., 2021, 2023).

HiPSCs were cultured at 37 °C (5% CO_2, 5% O_2) on Matrigel® -coated (Corning, 354 277) 6-well plates using mTeSR1 medium (Stem Cell Technologies, 83 850). At 80% confluence, the colonies were detached using Dispase (Stem Cell Technologies, 07923) and passaged in a 1:3 split ratio.

2.12. Differentiation of hiPSC-derived motoneurons

Motoneurons differentiation was carried out as previously described in Catanese et al., 2021). Briefly, hiPSC colonies were detached and cultivated in suspension in ultra-low attachment flasks T75 for 3 days for the formation of embryoid bodies (EBs) in hESC medium (DMEM/F12 + 20% knockout serum replacement + 1% NEAA + 1% β-mercaptoethanol + 1% antibiotic-antimycotic + SB-431542 10 μM + Dorsomorphin 1 μM + CHIR 99021 3 μM + Purmorphamine 1 μM + Ascorbic Acid 200 ng/μL + cAMP 10 μM + 1% B27 + 0.5% N2). On the fourth day, medium was switched to MN Medium (DMEM/F12 + 24 nM sodium selenite + 16 nM progesterone + 0.08 mg/mL apotransferrin +0.02 mg/mL insulin +7.72 μg/mL putrescine + 1% NEAA, 1% antibiotic-antimycotic + 50 mg/mL heparin +10 μg/mL of the neurotrophic factors BDNF, GDNF, and IGF-1, SB-431542 10 μM, Dorsomorphin 1 μM, CHIR 99021 3 μM, Purmorphamine 1 μM, Ascorbic Acid 200 ng/μL, Retinoic Acid 1 μM, cAMP 1 μM, 1% B27, 0.5% N2). Ultimately, after 5 further days of cultivation EBs were dissociated into single cells with Accutase (Sigma Aldrich) and plated onto μDishes, 24-well μPlates (Ibidi) or 6-well plates (Corning) pre-coated with Growth Factor Reduced Matrigel (Corning).

2.13. Data and statistical analysis

Data collection and statistical analysis were performed using Microsoft Excel and GraphPad Prism (Version 8).

All experiments with primary cells were performed in a minimum of N=3 independent replicates (independent preparations) and the following statistical tests were used: to compare two independent groups, unpaired *t*-test with Welch correction in case of normally distributed data, and nonparametric Mann-Whitney test in case of non-normal distribution; nonparametric ANOVA (Kruskal-Wallis test) followed by the Dunn's correction for multiple comparisons to evaluate differences among multiple groups; two-way ANOVA followed by the Holm-Šídák test for multiple comparisons was used to evaluate the effect of treatments on two independent experimental groups.

The experiments with hiPSC-derived neurons were performed in triplicates (independent differentiations) for each cell line. Since each line has been obtained from an individual and represents n=1, the average of the values obtained from all the neurons analyzed from the independent differentiations (after normalization to the vehicle treatment) was used to obtain a single value for each individual patient to perform statistical analysis (in order to compare the different genotypes or treatments). In this case, the effect of propranolol was evaluated performing a paired *t*-test.

The analysis of proteomic experiments was performed using DIA-NN software (version 1.8.1). A search against the rat UniProtKB Swiss-Prot/TrEMBL Rattus norvegicus database (release 02-2022, 52 910 entries) was performed using library free workflow. For this purpose, "FASTA digest for library free search/library generation" and "Deep learning spectra, RTs and IMs prediction" options were checked for precursor ion generation. Maximum of 1 trypsin missed cleavages was allowed and maximum variable modification was set to 2. Carbamidomethylation (Cys) was set as fixed modification, whereas protein N-terminal methionine excision, methionine oxidation and protein N-terminal acetylation were set as variable modifications. Peptide length range was set to 7-30 amino acids, precursor charge range 2-4, precursor m/z range 300-1800 and fragment ion m/z range 300-1800. To search parent mass and fragment ions, accuracy was was set to 10 ppm for each analysis. The false discovery rates (FDRs) at the protein and peptide level were set to 1%. Match between runs was allowed. For the quantification strategy, Robust LC (high precision) was used as advised in the software documentation, whereas default settings were kept for the other algorithm parameters.

Statistical and bioinformatic analysis, including heatmaps, profile plots and clustering were performed with Perseus software (version 1.6.15) freely available at www.perseus-framework.org. R/R Studio (R version 4.1.2 (www.R-project.org) and RStudio version 2021.09.1 (www.rstudio.com)) were used for batch effect correction. The pg_report matrix output by DIA-NN was used and intensities were log2 transformed for statistical analysis. For statistical comparison, we set four groups (GFP_propranolol, GFP_vehicle, polyGA_propranolol, polyGA_vehicle), each containing 3 independent replicates. We then filtered the data to keep only proteins with at least 3 valid values in at least one group. HarmonizR R package (version 0.0.0.9; Voß et al., 2022) was used to correct for batch effect using *harmonizR()* function with the ComBat algorithm and ComBat_mode was set to 1. Next, the data were imputed to fill missing data points by creating a Gaussian distribution of random numbers with a standard deviation of 30% relative to the standard deviation of the measured values and 1.8 standard deviation downshift of the mean to simulate the distribution of low signal values. Then, a Student t-test was performed between control groups (GFP_propranolol and GFP_vehicle) and case groups (polyGA_propranolol and polyGA_vehicle) with s0 = 0.1 and FDR = 0.05. Finally, in order to investigate the interaction between polyGA group and treatment group, 2-way ANOVA was performed using a 2-factor experimental design (presence of treatment; genotype) and proteins with an interference *p*-value <0.01 were retained. Enrichment analysis was performed with *Enrichr* (Chen et al., 2013), while protein-protein interaction analysis and visualization were carried out using *OmicsNet 2.0* (Zhou et al., 2022).

All the experiments were performed in n = 3 independent cultures and treatments. Data are displayed as mean ± SEM.

Ethics approval

All procedures with human material were in accordance with the ethical committee of the Ulm University (Nr.0148/2009 and 265/12) and in compliance with the guidelines of the Federal Government of Germany. All participants gave informed consent for the study. The use of human material was approved by the Declaration of Helsinki concerning Ethical Principles for Medical Research Involving Human Subjects.

Preparation of rat primary cells was allowed by the Permit Nr. O.103 of *Land Baden-Württemberg* (Germany), and performed in respect of the guidelines for the welfare of experimental animals issued by the German Federal Government and the Max Planck Society, and the ARRIVE guidelines.

3. Results

3.1. Accumulation of toxic poly(GA) aggregates detrimentally impairs ubiquitin-dependent catabolism in neurons

We employed a AAV9-poly(GA)$_{175}$-EGFP (henceforth poly(GA)) previously generated and characterized by our group (Catanese et al., 2021) to investigate how cytotoxic protein aggregates affect neuronal fitness in ALS/FTD. Overexpression of poly(GA), the most abundant HRE toxic product, leads to the accumulation of aberrant cytosolic aggregates, reduces dendritic arborization (Catanese et al., 2021), triggers neuronal apoptosis (Fig. S1) and induces ubiquitin sequestration (Fig. 1A) and accumulation (Fig. 1B) in primary rat cortical cultures. To further investigate the detrimental effect exerted by aggregate accumulation in neuronal cells, we analyzed the total proteome of EGFP- and poly(GA)-EGFP neurons. With this approach, we identified 1071 significantly-altered proteins (470 down- and 601 up-regulated; Fig. 1C) in poly(GA)+ cells when compared to those transduced with the control AAV9-EGFP. By performing enrichment analysis using the Gene Ontology (GO) *biological processes* database, we found a deep alteration in the ubiquitin-dependent catabolic mechanisms (Fig. 1D), highlighting that the levels of several proteins involved in these pathways were either significantly reduced or increased in comparison to EGFP + neurons. In

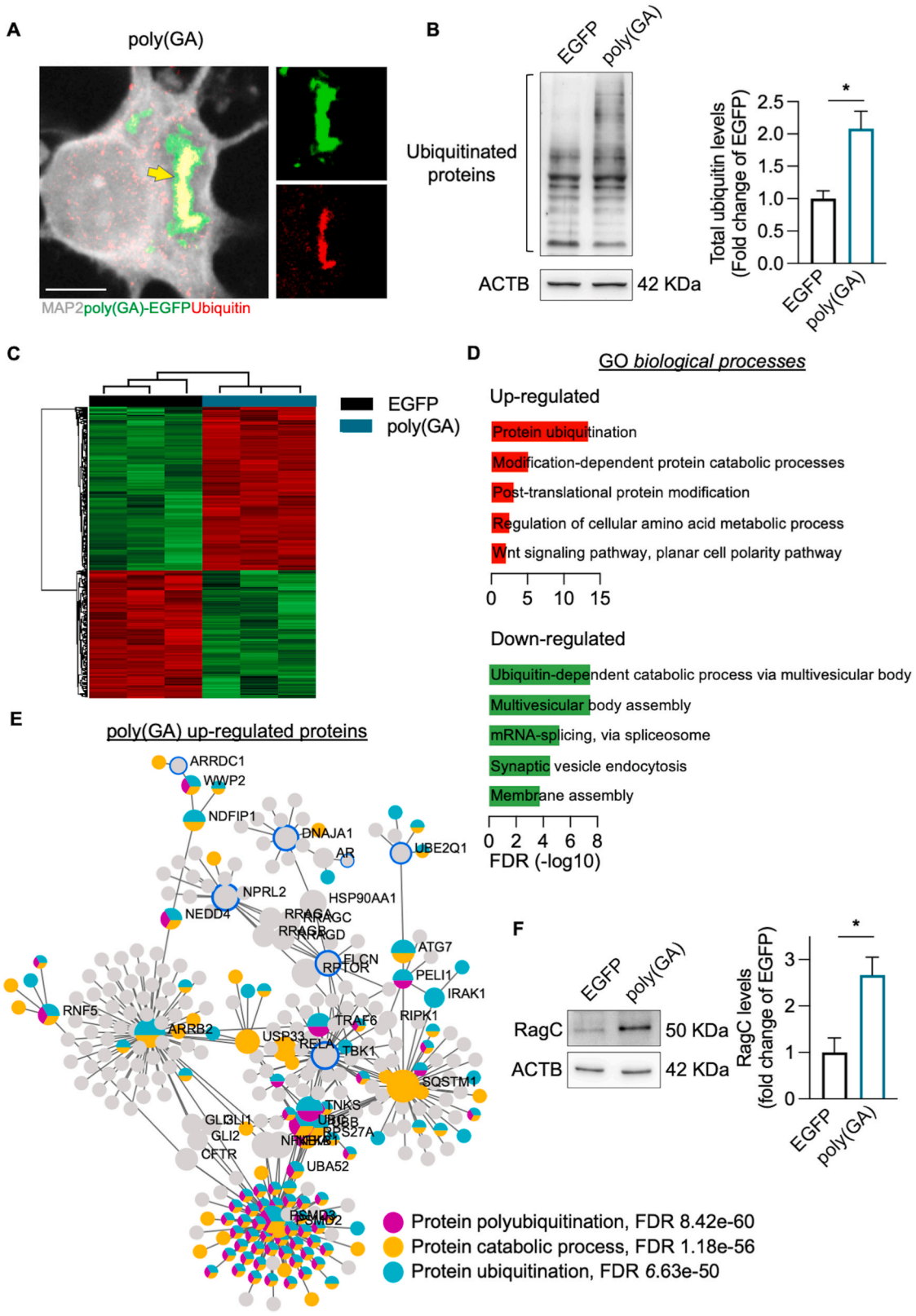

Fig. 1. Proteomic analysis of poly(GA)-expressing neurons highlights alterations in ubiquitin-dependent catabolism. (A) Representative confocal image showing sequestration of ubiquitin within poly(GA) aggregates. The yellow arrow indicates the poly(GA) aggregate sequestrating ubiquitin that has been displayed beside the composite picture. (B) Immunoblot analysis confirms significantly elevated levels of ubiquitinated proteins in poly(GA)+ neurons compared to EGFP + ones. (C) Heatmap representing the differentially expressed proteins in poly(GA)-expressing neurons vs. control EGFP + neurons. (D) GO (biological processes) terms of the top significant down- or up-regulated pathways in poly(GA)+ neurons. (E) Protein-protein interaction based on the clustering and distribution of the significantly up-regulated proteins in poly(GA)+ neurons. (F) Immunoblot analysis confirms higher levels of RagC in poly(GA)+ neurons compared to EGFP + ones. Scale bar in (A): 5 μm. In all experiments, n = 3 independent cultures; *p < 0.05. (For interpretation of the references to color in this figure legend, the reader is referred to the Web version of this article.)

fact, protein-protein interaction analysis identified a significant enrichment in proteins clustering into ubiquitination and catabolic processes (Fig. 1E), confirming a profound impairment in this specific arm of neuronal metabolism in the presence of poly(GA) aggregates. Interestingly, this bioinformatic approach highlighted also the enrichment of important interactors of C9orf72 within the poly (GA)-dependent interactome. The paralogs NPRL2 and FLCN (Figs. S2A–B), as well as the GTPase RagC (Fig. 1F), were indeed up-regulated in poly(GA)-expressing neurons, suggesting that the accumulation of toxic aggregates directly involves the disruption of the C9orf72-dependent autolysosomal machinery.

3.2. *Propranolol reduces the accumulation of cytotoxic aggregates and improves neuronal survival independently from autophagy in poly(GA)-transduced neurons*

The anti-hypertensive beta blocker propranolol has been previously shown to reduce the accumulation of amyloid and tau toxic species, as well as to improve cognitive alterations, in a mouse model of AD (Dobarro et al., 2013). Based on these observations, we asked whether this clinically approved drug might also exert a neuroprotective effect in our model of ALS/FTD. To this aim, we treated poly(GA) cultures with either DMSO (vehicle) or 10 μM propranolol for 24 h and assessed the burden of toxic aggregates. Microscopy analysis revealed that the treated neurons displayed a significantly lower accumulation of poly (GA)+ structures in comparison to the vehicle treated group (Fig. 2A). Importantly, the reduced burden appeared to be specific for this molecule since sotalol, another beta-blocker with reduced blood-brain barrier permeability than propranolol (Beaman et al., 2023), did not affect the accumulation of poly(GA) aggregates (Fig. S3).

The propranolol-dependent reduction of toxic aggregates correlated with an improved neuronal survival (as indicated by the lower number of cleaved caspase 3+ neurons; Fig. 2B), indicating a neuroprotective effect exerted by propranolol in this *in vitro* model of neurodegeneration. Accordingly, we confirmed the improved neuronal fitness upon propranolol treatment by observing that the signal intensity of the synaptic markers Synaptophysin and Homer1 along the dendrites was significantly higher in treated poly(GA) neurons than in the vehicle ones (Fig. S4).

We then asked whether the reduced accumulation of aggregates might result from improved catabolism, which was shown to be altered by the proteomic analysis. First, we performed qPCR with samples from vehicle- and propranolol-treated neurons to analyze the expression levels of EGFP and did not observe any significant difference between the two groups (Fig. S5). Since this ruled out a possible effect coming from reduced expression of the transgene, we next tested whether the neuroprotective effect exerted by propranolol might depend on macroautophagy, a major catabolic pathway. We first assessed the levels of SQSTM1/p62, which is sequestrated within poly(GA) aggregates (May et al., 2017), and found that propranolol significantly reduced the accumulation of this autophagy receptor (Fig. 2C). Afterwards, we investigated the effect of the beta blocker on the autophagic flux. In EGFP-expressing neurons, propranolol slightly increased the autophagosome-specific LC3-II form, whose levels were higher in

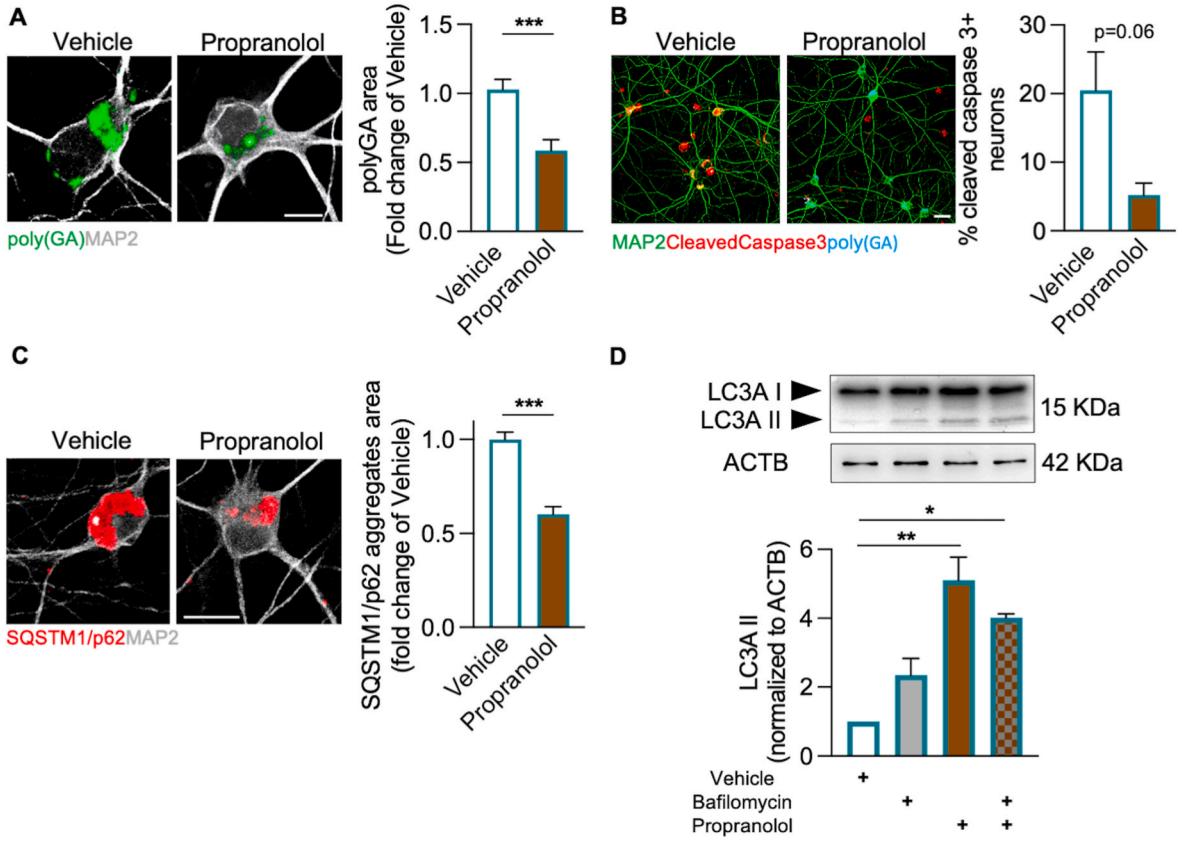

Fig. 2. Propranolol reduces aggregates' accumulation and improves neuronal survival in poly(GA) cultures. (A) Treatment of poly(GA) neurons with propranolol significantly decreases the aggregate burden in comparison to vehicle-treated cells. (B) Immunofluorescence analysis of the apoptotic marker cleaved caspase 3 reveals a significant decrease in neuronal death in poly(GA) cultures after propranolol treatment (p=0.06). (C) Propranolol reduces the accumulation of SQSTM1/p62 aggregates in ppoly(GA)-expressing neurons. (D) Analysis of autophagy dynamics upon treatment of poly(GA) neurons with bafilomycin A1, propranolol or both. Immunoblot against the autophagy-specific form LC3-II shows a late-phase blockade of the autophagic flux, as detected by the lack of additive effect on the autophagy marker in co-treated cultures. Scale bars in (A) and (B): 10 μm. Scale bar in (C): 15 μm. In all experiments, n = 3 treatments with independent cultures; *p < 0.05, **p < 0.01, ***p < 0.001.

bafilomycin-treated cultures and, in agreement with a flux induction (Mizushima and Yoshimori, 2007), further enhanced in co-treated neurons (Fig. S6). In disease-associated neurons we also detected a light LC3-II increase after propranolol treatment, while bafilomycin again induced LC3-II accumulation according to its canonical function (Klionsky et al., 2016). Interestingly, poly(GA) neurons did not display any additive effect on the levels of LC3-II upon co-treatment with propranolol and bafilomycin (Fig. 2D), which was indicative for a degradation blockade at the late steps of the autophagic flux (Mizushima and Yoshimori, 2007). Accordingly, we could not detect any increased colocalization between LC3A and the lysosomal marker LAMP1 in propranolol-treated poly(GA) neurons (Fig. S7). This suggested that propranolol enhances the autophagic flux in wild type neurons (as also previously observed in other models; Cammalleri et al., 2017), but fails to do so in cells loaded with toxic aggregates. Interestingly, propranolol treatment also did not increase the proteasomal activity in poly(GA) neurons (Fig. S8), indicating that both these major catabolic mechanisms are not responsible for the reduced accumulation of aggregates observed upon treatment with the beta blocker in this C9orf72-associated model.

3.3. *Increased levels of C9orf72 protein and lysosomal degradation are part of the neuroprotective effect of propranolol on poly(GA)-expressing neurons*

To elucidate the exact mechanisms by which propranolol induces the degradation of protein aggregates, we looked at the total proteome of EGFP- and poly(GA)-EGFP neurons treated with vehicle or the beta blocker. Using a stringent two-way ANOVA analysis (with a cutoff for significance set at p-value <0.01) we identified 165 significantly altered proteins that were grouped into 5 main clusters by hierarchical clustering (Fig. 3A). Interestingly, we noticed that the proteins grouped within the *blue cluster* displayed differential dynamics in EGFP and poly (GA) cultures upon treatment: while the levels of these proteins dropped below the values of vehicle-treated neurons in control cultures, they were significantly higher after propranolol exposure in the poly(GA)

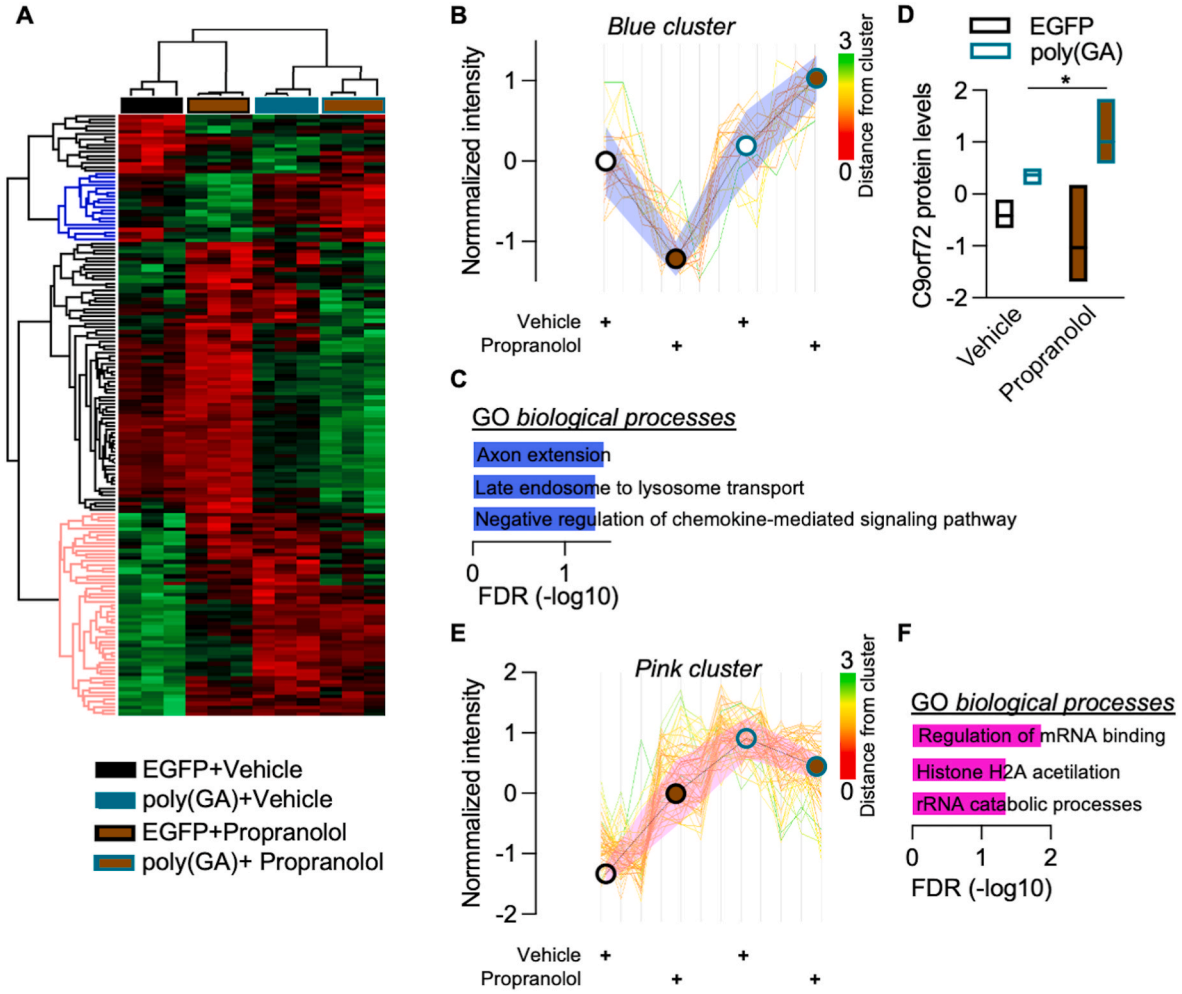

Fig. 3. Proteomic analysis reveals effects of propranolol on lysosomal dynamics and C9orf72 levels. (A) Heatmap representing the 165 significantly expressed proteins (two-way ANOVA, p<0.01) identified by proteomic analysis of poly(GA) an EGFP neurons treated with vehicle or propranolol. (B) Profile plot of the *blue cluster* displaying differential dynamics in EGFP and poly(GA) cultures upon propranolol treatment. The levels of the clustered proteins drop below the values of vehicle-treated neurons in control cultures, while they are significantly higher after propranolol exposure in the poly(GA) group. Single lines represent the proteins of the clustered, which are color-coded on the base of the distance from cluster (from red to green, closest to farthest). (C) GO (biological processes) enrichment analysis based on the blue cluster identifies terms related to axon extension, endo-lysosomal pathway and negative regulation of chemokine signaling. (D) Propranolol significantly elevates C9orf72 protein levels in poly(GA)+ neurons. (E) Profile plot of the *pink cluster*: clustered proteins are selectively increased in EGFP neurons by propranolol, while the beta blockers exerts the opposite effect in poly(GA) cultures (which have a higher baseline levels than controls). Single lines represent the proteins of the clustered, which are color-coded on the base of the distance from cluster (from red to green, closest to farthest). (F) GO (biological processes) groups the proteins of the pink cluster into mRNA metabolism and histone acetylation pathways. In all experiments, n = 3 treatments with independent cultures; *p < 0.05. (For interpretation of the references to color in this figure legend, the reader is referred to the Web version of this article.)

group (Fig. 3B). We found that the proteins grouped in these clustered were also involved in lysosomal degradation (Fig. 3C) and, most notably, included C9orf72, whose protein levels were up-regulated in poly(GA) neurons after propranolol treatment (Fig. 3D). In contrast, the proteins of the *pink cluster* showed an opposite trend than those of the *blue cluster*: their levels were increased in EGFP-expressing neurons upon propranolol treatment while being reduced by the same treatment in poly(GA) cultures (Fig. 3E). These proteins clustered into pathways related to mRNA metabolism (Fig. 3F), which has been widely described to be altered, but not exclusively, in the C9orf72 cases of ALS/FTD, suggesting a stabilization of different poly(GA)-related pathomechanisms after exposure to the beta blocker.

We then aimed to confirm the increased lysosomal activity highlighted by the proteomics experiment by analyzing the levels of LAMP1. We observed that poly(GA) neurons had a baseline of significantly lower number of lysosomes than EGFP controls and, confirming the proteome data, propranolol increased both the number and the signal intensity of LAMP1+ structures (Fig. 4A). In addition, by confocal microscopy we observed that the localization of the LAMP1 signal overlapped at significantly higher degrees with the poly(GA) aggregates upon propranolol treatment (Fig. 4B), suggesting local lysosomal activity. In fact, the lysosomal blocker E-64 completely abolished the degradation of poly (GA) structures induced by propranolol (Fig. 4C).

3.4. Propranolol reduces aggregate accumulation and improves the survival of C9orf72-mutant hiPSC-derived neuronal cultures

In order to gain more translational relevance on the potentially

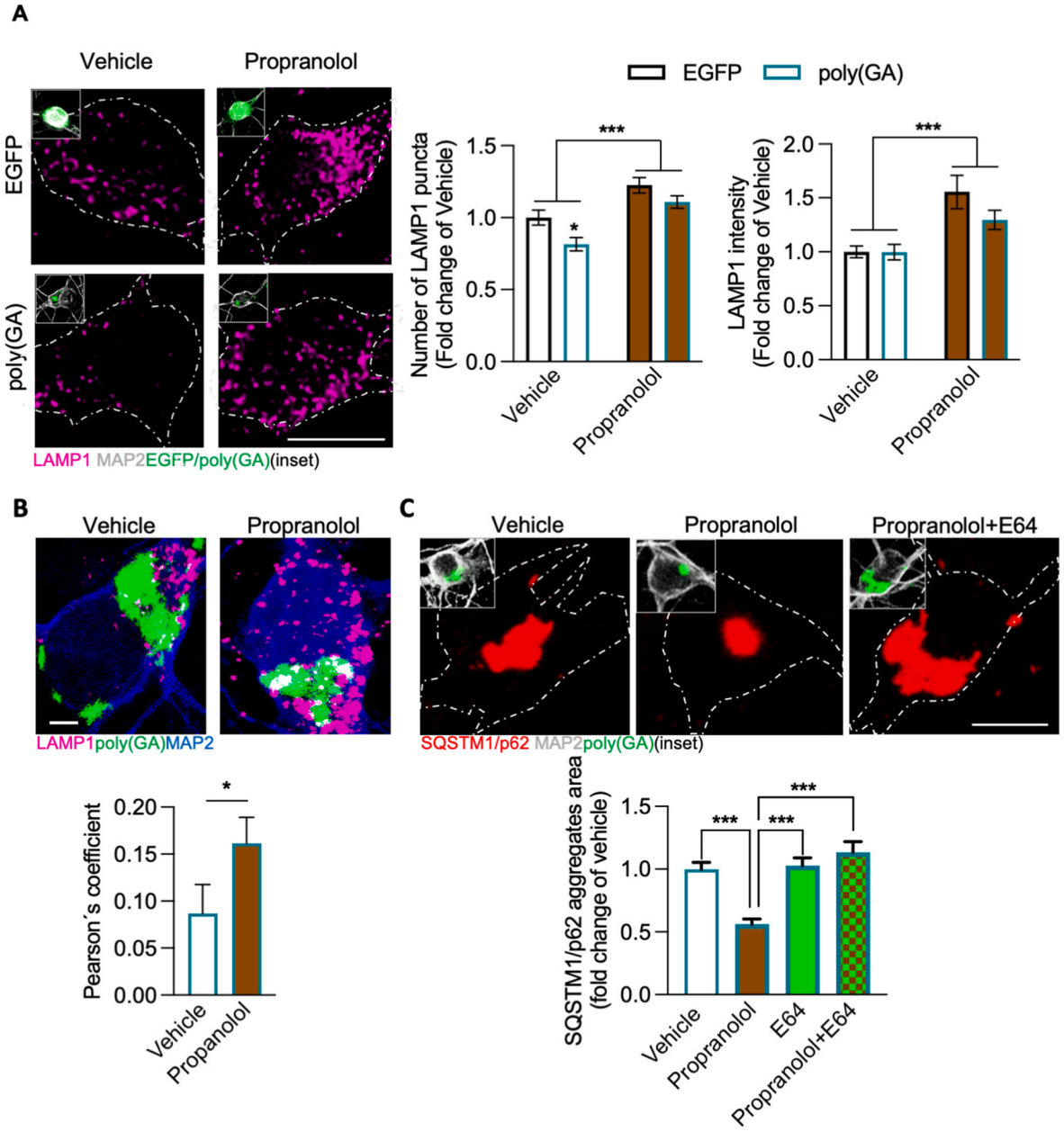

Fig. 4. Propranolol boosts lysosomal degradation in poly(GA) neurons. (A) Immunofluroescence analysis of the lysosomal marker LAMP1 shows a significantly decreased number of LAMP1 puncta in poly(GA) neurons compared to EGFP neurons. Upon treatment with propranolol, the number and intensity of LAMP1 puncta are increased both in poly(GA) as well as in EGFP cellss. (B) Representative confocal image showing increased colocalization of LAMP1 with poly(GA) aggregates upon propranolol treatment. (C) The lysosome blocker E-64 prevents the propranolol-dependent degradation of poly(GA) aggregates. Scale bars in (A) and (C): 10 μm. Scale bar in (B): 3 μm In all experiments, n = 3 treatments with independent cultures; *p < 0.05, ***p < 0.001.

beneficial effect of increased lysosomal degradation in ALS/FTD, we treated human iPSC-derived mutant motoneurons (MNs) with propranolol. We considered hiPSCs derived from 3 patients characterized by HRE within the *C9orf72* gene (Fig. 5A). Our group previously showed that these cells display the accumulation of aberrant SQSTM1/p62 aggregates and are characterized by a time-dependent increase in neuronal death (Catanese et al., 2021). We cultured the hiPSC-MNs for 9 weeks and treated mature neurons with propranolol for 24 h. Notably, we observed that propranolol treatment significantly reduced the SQSTM1/p62 burden (Fig. 5B) as well as the number of apoptotic cleaved caspase 3+ neurons (Fig. 5C) in the cultures derived from all the 3 patients.

Since the proteomic analysis revealed a selective increase of the C9orf72 protein levels in poly(GA) neurons after treatment with propranolol, we asked whether this might hold true also in our human model. First, we looked at the expression of C9orf72 using a RNAseq dataset previously published by our group (Catanese et al., 2021; GSE168831) that included 2 of the ALS^{C9orf72} lines considered in this study and compared them to a healthy patient and an isogenic control (referred to as Healthy). Confirming the idea that C9orf72 haploinsufficiency contributes to ALS pathogenesis (Shi et al., 2018), we found significantly lower levels of its transcript in the ALS^{C9orf72}-mutant MNs than in Healthy ones (Fig. 5D). Notably, we found that MNs from ALS patients (Fig. 5E), as well as from healthy controls (Fig. S9), displayed a clear trend toward increased protein levels of C9orf72 after treatment with the beta blocker. This suggested that the propranolol-dependent neuroprotective induction of catabolic processes, which reduce the accumulation of cytotoxic aggregates in ALS neurons, includes C9orf72 protein itself.

4. Discussion

Targeting catabolic pathways has been often indicated as a valid strategy for the development of novel therapies against neurodegenerative diseases. In fact, several proof-of-principle studies focusing on different neurological disorders have shown that increasing autophagic, proteasomal or endo-lysosomal degradation effectively reduces the accumulation of cytotoxic aggregates, re-establishes physiological homeostasis and neurons from high levels of intracellular stress. The heterogenic aggregates' composition appears indeed to affect not only

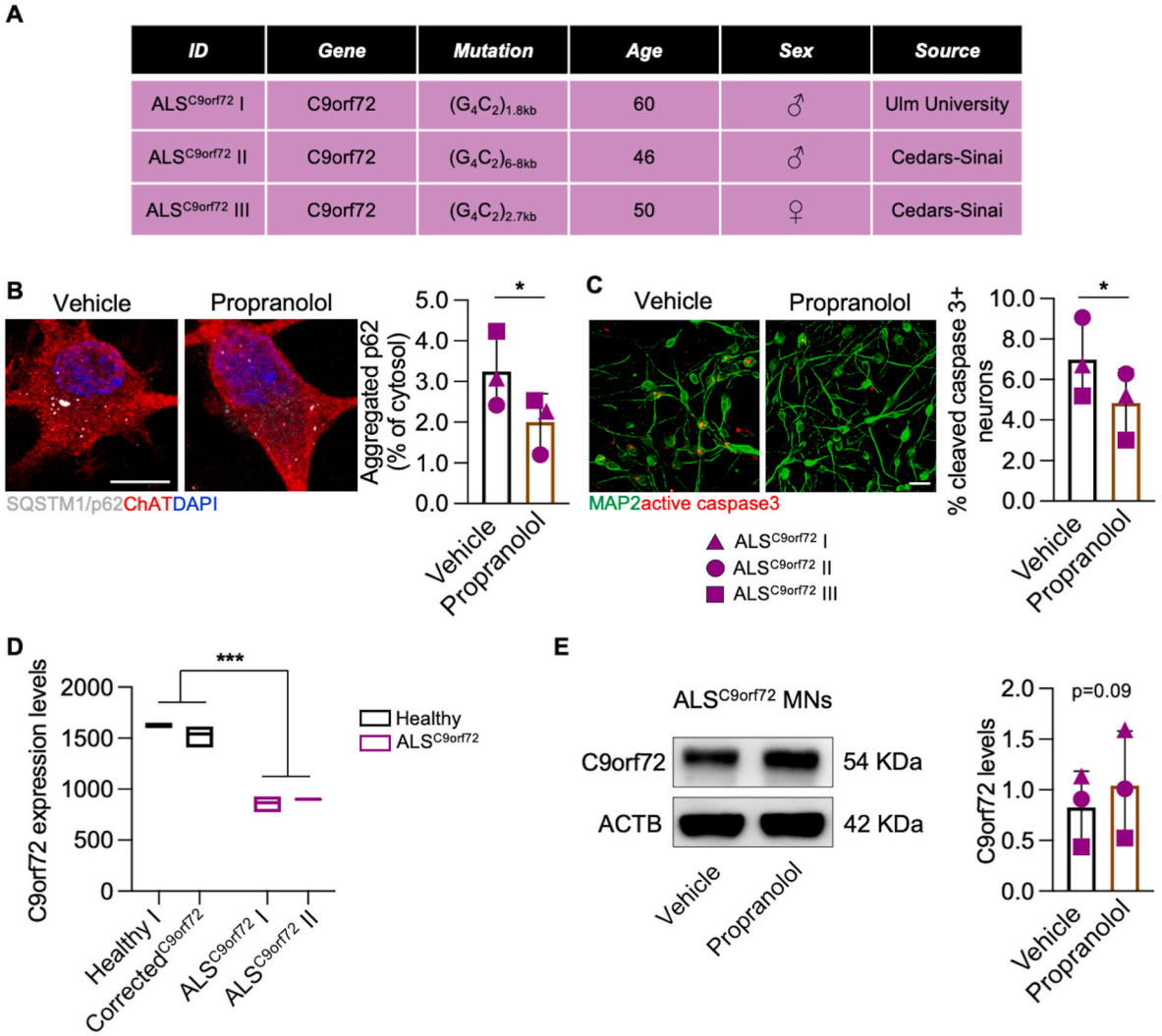

Fig. 5. Propranolol treatment rescues aggregate burden and neuronal death in hiPSC-derived ALS^{C9orf72} MNs. (A) List of the mutant hiPSC lines used in this study. (B) hiPSC-derived MNs show a significant reduction of SQSTM1/p62+ aggregates after propranolol treatment. Values are represented as mean ± SEM, significance was tested using paired *t*-test (n = 3 independent treatments with each hiPSC line). (C) Propranolol treatment improves neuronal survival in hiPSC MN cultures. (D) ALS^{C9orf72}-mutant MNs have significantly lower expression levels of C9orf72 RNA than Healthy ones (analysis based on the transcriptome published in Catanese et al., 2021). (E) Immunoblot analysis shows a trend (p=0.09) toward increased C9orf72 protein levels in C9orf72-mutant MNs after propranolol treatment. Scale bars: 10 μm. In all experiments, n = 3 treatments with independent cultures; *p < 0.05, ***p < 0.001.

degradative mechanisms, but also several other important cellular pathways such as synaptic activity and transport (Catanese et al., 2021; Baron et al., 2022). Accordingly, beside inducing the accumulation of ubiquitinated proteins (which indicates degradative impairment), poly (GA) overexpression significantly altered the levels of proteins involved, among others, in mRNA and amino acid metabolism, Wnt signaling and synaptic composition. This confirmed that the accumulation of such aberrant structures *per se* is sufficient to trigger in healthy neurons, some of the typical pathologic features observed in ALS/FTD (May et al., 2017) that can be rescued by reducing the aggregates load in neuronal cells. In fact, propranolol ameliorated the overall fitness of poly(GA) and $ALS^{C9orf72}$ neurons, as demonstrated by the increased levels of the synaptic proteins and the improved survival observed upon treatment. Accordingly, RNAseq experiments have shown that propranolol treatment modifies the expression of genes involved in neuronal survival and axon guidance (Castonguay et al., 2022), which supports the specific effect exerted by this molecule in poly(GA) neurons that was highlighted by the *blue cluster* of our proteomic analysis. These results also revealed that the beta blocker, in line with its lysosomotropic properties (Müller et al., 2020), triggers lysosomal degradation to efficiently reduce the aggregates accumulating within ALS-related neurons without influencing macroautophagy or proteasomal activity. Since other molecules with similar biochemical properties have already been shown to ameliorate disease phenotypes in neurodegeneration (Vest et al., 2022), this might represent a valid alternative to reduce neuronal stress in ALS/FTD instead of boosting the canonical autophagic flux. Several groups have indeed shown that enhancing autophagic degradation exacerbates, instead of resolving, the degradative impairments that characterize vulnerable neurons. For example, treating the SOD1G93A mouse with autophagy inducers such as rapamycin or rilmenidine worsens the disease progression in this animal model of ALS (Zhang et al., 2011; Saxena et al., 2013; Perera et al., 2018). In contrast, independent pieces of evidence highlighted therapeutic potential for chemicals enhancing catabolic pathways as drugs inducing autophagy tested beneficial, among others, in FUS and C9orf72 human *in vitro* models (Marrone et al., 2018; Licata et al., 2022). This controversy on the effectiveness of enhanced degradation in ALS is even worsened when considering some of the genetic causes of this disease, which are genes directly involved in the autophagic pathway (reviewed by Nguyen et al., 2019). Thus, mutations in genes such as TBK1 or SQSTM1 have a direct detrimental effect on the efficiency of the autophagic flux and lead to intrinsic autophagy blockades, which contribute to the accumulation of cytotoxic aggregates and that require to be addressed before increasing degradation (Catanese et al., 2019; Deng et al., 2020). In the specific case of C9orf72, its role in cellular catabolism has been described in both autophagic and endolysosomal proteostasis (Sellier et al., 2016 Shi et al., 2018. In both cases, it was shown that this protein is required at the early phase of the catabolic mechanisms where it contributes to the formation of the degradative compartment (Sellier et al., 2016; Webster et al., 2016; Amick et al., 2020). Mechanistically, it has been demonstrated that C9orf72 interacts with several members of the Rab family (Sellier et al., 2016; Webster et al., 2016; Aoki et al., 2017), which are involved in canonical and, at least partially, non-canonical autophagy (Nishida et al., 2009). This latter form of macroautophagy has been shown to not necessarily rely on ubiquitin-like conjugation proteins such as Atg5, Atg7 and LC3 to support the formation of lysosomal compartments (Codogno et al., 2011). Notably, we identified a detrimental up-regulation of the C9orf72 paralogs NPRL2 and FLCN, as well as of the GTPase RagC, in poly(GA)-expressing neurons. These proteins are important regulators of lysosomal biogenesis involving mTORC1-dependent signaling (Shen et al., 2017, 2019) and their accumulation in the presence of cytotoxic aggregates suggests a profound alteration of the catabolic machinery that does not solely affects the C9orf72-SMCR8 complex (Sellier et al., 2016). Still, propranolol efficiently reduced the accumulation of poly(GA) structures despite the underlying blockade of the autophagic flux. This suggests that alternative and non-canonical forms of catabolic processes might represent a valid strategy to overcome the degradative blockades that lead to autophagic overload in ALS (Catanese et al., 2019). In fact, despite propranolol could activate the autophagic flux in control but not in poly(GA) neurons, we could detect higher levels of lysosomes in both experimental groups after treatment, strengthening the idea of unconventional degradative pathways activated by the beta blocker in disease-associated cultures. Although the molecular mechanisms behind this specific effect of propranolol still have to be dissected, a possible explanation is the recruitment and activation of Rab9-dependent non-conventional autophagy (Nishida et al., 2009). This monomeric GTPase, in contrast to other members of the same family, does not appear to neither interact with nor being involved in the catabolic signaling cascade related to C9orf72 (Webster et al., 2018), supporting the idea that this pathway might efficiently increase degradation without being limited by the underlying impairments deriving from pathogenic mutations. In fact, Rab9 directly controls lysosome biogenesis (Riederer et al., 1994).

For completeness, it has to be mentioned that lysosomotropic drugs have been shown to induce the phosphorylation of Rab10, which is involved in the maturation of the phagosome, as a result of increased Rab29(Rab7L1)-mediated activation of the PD-related protein LRRK2 (Kuwahara et al., 2020). Notably, Rab10 and other members of the Rab8 subfamily interact with C9orf72 (Sellier et al., 2016; Frick et al., 2018) and propranolol increased the C9orf72 protein levels. Thus, it is reasonable to speculate that enhanced functionality of specific Rab-members might trigger a positive feedback loop activating several interactors of these proteins including C9orf72 itself. This aspect, which still has to be experimentally proven, represents an intriguing possibility to beneficially improve the effectiveness of degradative mechanisms in the presence of C9orf72 mutations. An important finding highlighted in this work is in fact the potential detrimental synergism between loss- and toxic gain-of-function related to C9orf72 pathology. Indeed, while the presence of HRE results in the accumulation of cytotoxic RNA foci and DPRs (DeJesus-Hernandez et al., 2011), reduced expression of C9orf72 impairs the autophagic flux by limiting the maturation of the phagophore (Webster et al., 2018). Interestingly, several groups have aimed at targeting the deposition of DPRs and RNA foci with heterogeneous methods such as small molecules, antibodies, CRISPR-Cas9 editing and antisense oligonucleotides (Zhou et al., 2017; Czuppa et al., 2022; Meijboom et al., 2022; Tran et al., 2022), speculating that this aspect of HRE pathology might be prioritized when developing therapeutic strategies. Indeed, C9orf72 haploinsufficiency has been inconsistently reported (Shi et al., 2018; Sareen et al., 2013). Unfortunately, the recently discontinued clinical trial of the antisense oligonucleotides targeting C9orf72 suggests that the disease mechanisms associated to this mutation cannot only be explained by the toxic products of the hexanucleotide expansion and that the dosage and functionality of the native C9orf72 protein should be addressed as well. Accordingly, its levels were increased by propranolol, confirming the role of this protein in lysosomal activity and highlighting an important interplay between the accumulation of toxic DPRs and their efficient lysosomal degradation. The significance of these findings is further strengthened by the work of Zhu and colleagues, who observed increased disease severity and progression when silencing the C9orf72 gene in the presence of DPRs (Zhu et al., 2020). Of note, the presence of the genetic mutation in our human model, which display significantly lower levels of C9orf72 mRNA in comparison to healthy and isogenic controls (Catanese et al., 2021), might explain the reduced magnitude of propranolol effect in comparison to the overexpression of poly(GA) in primary neurons. Nevertheless, this study highlights an important correlation between both sides of C9orf72-related pathology, which appear to create a pathologic vicious circle if not efficiently addressed at the same time.

Funding

This work was founded from the Bausteinprogramm of the Medical Faculty of Ulm University to AC (project L.SBN.0162).

TB and AC are supported by the Deutsche Forschungsgemeinschaft (German Research Foundation) - SFB1506 "Aging at interfaces" (project A01). AC is also supported by the Else Kröner-Fresenius Stiftung (project Nr. 2019_A111) and the Frick Foundation.

MS and CS received financial support from the "Experimental Medicine" graduate program of the Medical Faculty of Ulm University.

CRediT authorship contribution statement

Mira Seidel: Data curation, Formal analysis, Investigation, Methodology, Visualization, Writing – original draft. **Sandeep Rajkumar:** Formal analysis, Investigation, Methodology, Writing – original draft. **Christina Steffke:** Formal analysis, Investigation, Methodology, Visualization. **Vivien Noeth:** Methodology. **Shreya Agarwal:** Methodology. **Kevin Roger:** Formal analysis. **Joanna Lipecka:** Methodology. **Albert Ludolph:** Supervision. **Chiara Ida Guerrera:** Formal analysis, Investigation, Visualization. **Tobias Boeckers:** Resources, Writing – original draft. **Alberto Catanese:** Conceptualization, Formal analysis, Funding acquisition, Project administration, Resources, Supervision, Visualization, Writing – final version.

Declaration of competing interest

The authors declare that they have no known competing financial interests or personal relationships that could have appeared to influence the work reported in this paper.

Data availability

Data will be made available on request.

Acknowledgements

The authors are thankful to Maria Manz and Sabine Seltenheim for the valuable technical support.

Appendix A. Supplementary data

Supplementary data to this article can be found online at https://doi.org/10.1016/j.crneur.2023.100105.

References

Amick, J., Tharkeshwar, A.K., Talaia, G., Ferguson, S.M., 2020. PQLC2 recruits the C9orf72 complex to lysosomes in response to cationic amino acid starvation. J. Cell Biol. 219 (1) https://doi.org/10.1083/JCB.201906076.

Aoki, Y., Manzano, R., Lee, Y., Dafinca, R., Aoki, M., Douglas, A.G.L., Varela, M.A., Sathyaprakash, C., Scaber, J., Barbagallo, P., Vader, P., Mäger, I., Ezzat, K., Turner, M.R., Ito, N., Gasco, S., Ohbayashi, N., el Andaloussi, S., Takeda, S., et al., 2017. C9orf72 and RAB7L1 regulate vesicle trafficking in amyotrophic lateral sclerosis and frontotemporal dementia. Brain : J. Neurol. 140 (4), 887–897. https://doi.org/10.1093/BRAIN/AWX024.

Baron, D.M., Fenton, A.R., Saez-Atienzar, S., Giampetruzzi, A., Sreeram, A., Shankaracharya, Keagle, P.J., Doocy, V.R., Smith, N.J., Danielson, E.W., Andresano, M., McCormack, M.C., Garcia, J., Bercier, V., van den Bosch, L., Brent, J. R., Fallini, C., Traynor, B.J., Holzbaur, E.L.F., Landers, J.E., 2022. ALS-associated KIF5A mutations abolish autoinhibition resulting in a toxic gain of function. Cell Rep. 39 (1) https://doi.org/10.1016/J.CELREP.2022.110598.

Beaman, E.E., Bonde, A.N., Larsen, S.M.U., Ozenne, B., Lohela, T.J., Nedergaard, M., Gíslason, G.H., Knudsen, G.M., Holst, S.C., 2023. Blood-brain barrier permeable β-blockers linked to lower risk of Alzheimer's disease in hypertension. Brain 146 (3), 1141–1151. https://doi: 10.1093/brain/awac076.

Belzil, V.v., Bauer, P.O., Prudencio, M., Gendron, T.F., Stetler, C.T., Yan, I.K., Pregent, L., Daughrity, L., Baker, M.C., Rademakers, R., Boylan, K., Patel, T.C., Dickson, D.W., Petrucelli, L., 2013. Reduced C9orf72 gene expression in c9FTD/ALS is caused by histone trimethylation, an epigenetic event detectable in blood. Acta Neuropathol. 126 (6), 895–905. https://doi.org/10.1007/S00401-013-1199-1.

Boivin, M., Pfister, V., Gaucherot, A., Ruffenach, F., Negroni, L., Sellier, C., Charlet-Berguerand, N., 2020. Reduced autophagy upon C9ORF72 loss synergizes with dipeptide repeat protein toxicity in G4C2 repeat expansion disorders. EMBO J. 39 (4) https://doi.org/10.15252/embj.2018100574.

Brasseur, L., Coens, A., Waeytens, J., Melki, R., Bousset, L., 2020. Dipeptide repeat derived from C9orf72 hexanucleotide expansions forms amyloids or natively unfolded structures in vitro. Biochem. Biophys. Res. Commun. 526 (2), 410–416. https://doi.org/10.1016/J.BBRC.2020.03.108.

Burrell, J.R., Halliday, G.M., Kril, J.J., Ittner, L.M., Götz, J., Kiernan, M.C., Hodges, J.R., 2016. The frontotemporal dementia-motor neuron disease continuum. Lancet (London, England) 388 (10047), 919–931. https://doi.org/10.1016/S0140-6736(16)00737-6.

Cammalleri, M., Locri, F., Catalani, E., Filippi, L., Cervia, D., Dal Monte, M., Bagnoli, P., 2017. The beta adrenergic receptor blocker propranolol counteracts retinal dysfunction in a mouse model of oxygen induced retinopathy: restoring the balance between apoptosis and autophagy. Front. Cell. Neurosci. 11, 395. https://doi.org/10.3389/FNCEL.2017.00395/BIBTEX.

Castonguay, C.E., Liao, C., Khayachi, A., Liu, Y., Medeiros, M., Houle, G., Ross, J.P., Dion, P.A., Rouleau, G.A., 2022. Transcriptomic effects of propranolol and primidone converge on molecular pathways relevant to essential tremor. Npj Genomic Medicine 7 (1), 1–13. https://doi.org/10.1038/s41525-022-00318-9, 2022 7:1.

Catanese, A., Olde Heuvel, F., Mulaw, M., Demestre, M., Higelin, J., Barbi, G., Freischmidt, A., Weishaupt, J.H., Ludolph, A.C., Roselli, F., Boeckers, T.M., 2019. Retinoic acid worsens ATG10-dependent autophagy impairment in TBK1-mutant hiPSC-derived motoneurons through SQSTM1/p62 accumulation. Autophagy 15 (10), 1719–1737. https://doi.org/10.1080/15548627.2019.1589257.

Catanese, A., Rajkumar, S., Sommer, D., Freisem, D., Wirth, A., Aly, A., Massa-López, D., Olivieri, A., Torelli, F., Ioannidis, V., Lipecka, J., Guerrera, I.C., Zytnicki, D., Ludolph, A., Kabashi, E., Mulaw, M.A., Roselli, F., Böckers, T.M., 2021. Synaptic disruption and CREB-regulated transcription are restored by K+ channel blockers in ALS. EMBO Mol. Med. 13 (7) https://doi.org/10.15252/EMMM.202013131.

Catanese, A., Rajkumar, S., Sommer, D., Masrori, P., Hersmus, N., Van Damme, P., Witzel, S., Ludolph, A., Ho, R., Boeckers, T.M., Mulaw, M., 2023. Multiomics and machine-learning identify novel transcriptional and mutational signatures in amyotrophic lateral sclerosis. Brain. https://doi.org/10.1093/brain/awad075 awad075.

Chang, Y.J., Jeng, U.S., Chiang, Y.L., Hwang, I.S., Chen, Y.R., 2016. The glycine-alanine dipeptide repeat from C9orf72 hexanucleotide expansions forms toxic amyloids possessing cell-to-cell transmission properties. J. Biol. Chem. 291 (10), 4903–4911. https://doi.org/10.1074/JBC.M115.694273.

Chen, E.Y., Tan, C.M., Kou, Y., Duan, Q., Wang, Z., Meirelles, G.V., Clark, N.R., Ma'ayan, A., 2013. Enrichr: interactive and collaborative HTML5 gene list enrichment analysis tool. BMC Bioinf. 128 (14). https://doi: 10.1186/1471-2105-14-128.

Cheng, C.W., Lin, M.J., Shen, C.K.J., 2015. Rapamycin alleviates pathogenesis of a new Drosophila model of ALS-TDP. J. Neurogenet. 29 (2–3), 59–68. https://doi.org/10.3109/01677063.2015.1077832.

Codogno, P., Mehrpour, M., Proikas-Cezanne, T., 2011. Canonical and non-canonical autophagy: variations on a common theme of self-eating? Nat. Rev. Mol. Cell Biol. 13 (1), 7–12. https://doi.org/10.1038/nrm3249.

Czuppa, M., Dhingra, A., Zhou, Q., Schludi, C., König, L., Scharf, E., Farny, D., Dalmia, A., Täger, J., Castillo-Lizardo, M., Katona, E., Mori, K., Aumer, T., Schelter, F., Müller, M., Carell, T., Kalliokoski, T., Messinger, J., Rizzu, P., et al., 2022. Drug screen in iPSC-Neurons identifies nucleoside analogs as inhibitors of (G4C2)n expression in C9orf72 ALS/FTD. Cell Rep. 39 (10) https://doi.org/10.1016/j.celrep.2022.110913.

DeJesus-Hernandez, M., Mackenzie, I.R., Boeve, B.F., Boxer, A.L., Baker, M., Rutherford, N.J., Nicholson, A.M., Finch, N.C.A., Flynn, H., Adamson, J., Kouri, N., Wojtas, A., Sengdy, P., Hsiung, G.Y.R., Karydas, A., Seeley, W.W., Josephs, K.A., Coppola, G., Geschwind, D.H., et al., 2011. Expanded GGGGCC hexanucleotide repeat in noncoding region of C9ORF72 causes chromosome 9p-linked FTD and ALS. Neuron 72 (2), 245–256. https://doi.org/10.1016/J.NEURON.2011.09.011.

Deng, Z., Lim, J., Wang, Q., Purtell, K., Wu, S., Palomo, G.M., Tan, H., Manfredi, G., Zhao, Y., Peng, J., Hu, B., Chen, S., Yue, Z., 2020. ALS-FTLD-linked mutations of SQSTM1/p62 disrupt selective autophagy and NFE2L2/NRF2 anti-oxidative stress pathway. Autophagy 16 (5), 917–931. https://doi.org/10.1080/15548627.2019.1644076.

Dobarro, M., Gerenu, G., Ramírez, M.J., 2013. Propranolol reduces cognitive deficits, amyloid and tau pathology in Alzheimer's transgenic mice. Int. J. Neuropsychopharmacol. 16 (10), 2245–2257. https://doi.org/10.1017/S1461145713000631.

Edbauer, D., Haass, C., 2016. An amyloid-like cascade hypothesis for C9orf72 ALS/FTD. Curr. Opin. Neurobiol. 36, 99–106. https://doi.org/10.1016/J.CONB.2015.10.009.

Farg, M.A., Sundaramoorthy, V., Sultana, J.M., Yang, S., Atkinson, R.A.K., Levina, V., Halloran, M.A., Gleeson, P.A., Blair, I.P., Soo, K.Y., King, A.E., Atkin, J.D., 2014. C9ORF72, implicated in amytrophic lateral sclerosis and frontotemporal dementia, regulates endosomal trafficking. Hum. Mol. Genet. 23 (13), 3579–3595. https://doi.org/10.1093/HMG/DDU068.

Frick P, Sellier C, Mackenzie IRA, Cheng CY, Tahraoui-Bories J, Martinat C, Pasterkamp RJ, Prudlo J, Edbauer D, Oulad-Abdelghani M, Feederle R, Charlet-Berguerand N, Neumann M. Novel antibodies reveal presynaptic localization of C9orf72 protein and reduced protein levels in C9orf72 mutation carriers. Acta Neuropathol Commun. 2018 Aug 3;6(1):72. doi: 10.1186/s40478-018-0579-0.

Gijselinck, I., van Mossevelde, S., van der Zee, J., Sieben, A., Engelborghs, S., de Bleecker, J., Ivanoiu, A., Deryck, O., Edbauer, D., Zhang, M., Heeman, B.,

Bäumer, V., van den Broeck, M., Mattheijssens, M., Peeters, K., Rogaeva, E., de Jonghe, P., Cras, P., Martin, J.J., et al., 2016. The C9orf72 repeat size correlates with onset age of disease, DNA methylation and transcriptional downregulation of the promoter. Mol. Psychiatr. 21 (8), 1112–1124. https://doi.org/10.1038/MP.2015.159.

Ho, W.Y., Tai, Y.K., Chang, J.C., Liang, J., Tyan, S.H., Chen, S., Guan, J.L., Zhou, H., Shen, H.M., Koo, E., Ling, S.C., 2019. The ALS-FTD-linked gene product, C9orf72, regulates neuronal morphogenesis via autophagy. Autophagy 15 (5), 827–842. https://doi.org/10.1080/15548627.2019.1569441.

Khosravi, B., LaClair, K.D., Riemenschneider, H., Zhou, Q., Frottin, F., Mareljic, N., Czuppa, M., Farny, D., Hartmann, H., Michaelsen, M., Arzberger, T., Hartl, F.U., Hipp, M.S., Edbauer, D., 2020. Cell-to-cell transmission of C9orf72 poly-(Gly-Ala) triggers key features of ALS/FTD. EMBO J. 39 (8) https://doi.org/10.15252/EMBJ.2019102811.

Klionsky, D.J., Abdelmohsen, K., Abe, A., Abedin, M.J., Abeliovich, H., Arozena, A.A., Adachi, H., Adams, C.M., Adams, P.D., Adeli, K., Adhihetty, P.J., Adler, S.G., Agam, G., Agarwal, R., Aghi, M.K., Agnello, M., Agostinis, P., Aguilar, P.v., Aguirre-Ghiso, J., et al., 2016. Guidelines for the use and interpretation of assays for monitoring autophagy (3rd edition). In: Autophagy, 12. Taylor and Francis Inc, pp. 1–222. https://doi.org/10.1080/15548627.2015.1100356, 1.

Kuwahara, T., Funakawa, K., Komori, T., Sakurai, M., Yoshii, G., Eguchi, T., Fukuda, M., Iwatsubo, T., 2020. Roles of lysosomotropic agents on LRRK2 activation and Rab10 phosphorylation. Neurobiol. Dis. 145, 105081 https://doi.org/10.1016/J.NBD.2020.105081.

Levine, T.P., Daniels, R.D., Gatta, A.T., Wong, L.H., Hayes, M.J., 2013. The product of C9orf72, a gene strongly implicated in neurodegeneration, is structurally related to DENN Rab-GEFs. Bioinformatics 29 (4), 499–503. https://doi.org/10.1093/BIOINFORMATICS/BTS725.

Licata, N. v, Cristofani, R., Salomonsson, S., Wilson, K.M., Kempthorne, L., Vaizoglu, D., D'Agostino, V.G., Pollini, D., Loffredo, R., Pancher, M., Adami, V., Bellosta, P., Ratti, A., Viero, G., Quattrone, A., Isaacs, A.M., Poletti, A., Provenzani, A., 2022. C9orf72 ALS/FTD dipeptide repeat protein levels are reduced by small molecules that inhibit PKA or enhance protein degradation. EMBO J. 41 (1) https://doi.org/10.15252/EMBJ.2020105026.

Maduro, M.F., Gordon, M., Jacobs, R., Pilgrim, D.B., 2000. The UNC-119 family of neural proteins is functionally conserved between humans, Drosophila and C. elegans. J. Neurogenet. 13 (4), 191–212. https://doi.org/10.3109/01677060009084494.

Marrone, L., Poser, I., Casci, I., Japtok, J., Reinhardt, P., Janosch, A., Andree, C., Lee, H. O., Moebius, C., Koerner, E., Reinhardt, L., Cicardi, M.E., Hackmann, K., Klink, B., Poletti, A., Alberti, S., Bickle, M., Hermann, A., Pandey, U.B., et al., 2018. Isogenic FUS-eGFP iPSC reporter lines enable quantification of FUS stress granule pathology that is rescued by drugs inducing autophagy. Stem Cell Rep. 10 (2), 375–389. https://doi.org/10.1016/j.stemcr.2017.12.018.

May, S., Hornburg, D., Schludi, M.H., Arzberger, T., Rentzsch, K., Schwenk, B.M., Grässer, F.A., Mori, K., Kremmer, E., Banzhaf-Strathmann, J., Mann, M., Meissner, F., Edbauer, D., 2014. C9orf72 FTLD/ALS-associated Gly-Ala dipeptide repeat proteins cause neuronal toxicity and Unc119 sequestration. Acta Neuropathol. 128 (4), 485–503. https://doi.org/10.1007/S00401-014-1329-4.

Meijboom, K.E., Abdallah, A., Fordham, N.P., Nagase, H., Rodriguez, T., Kraus, C., Gendron, T.F., Krishnan, G., Esanov, R., Andrade, N.S., Rybin, M.J., Ramic, M., Stephens, Z.D., Edraki, A., Blackwood, M.T., Kahriman, A., Henninger, N., Kocher, J.-P.A., Benatar, M., et al., 2022. CRISPR/Cas9-mediated excision of ALS/FTD-causing hexanucleotide repeat expansion in C9ORF72 rescues major disease mechanisms in vivo and in vitro. Nat. Commun. 13 (1), 6286. https://doi.org/10.1038/s41467-022-33332-7.

Mizushima, N., Yoshimori, T., 2007. How to interpret LC3 immunoblotting. Autophagy 3 (6), 542–545. https://doi.org/10.4161/auto.4600.

Mori, K., Weng, S.M., Arzberger, T., May, S., Rentzsch, K., Kremmer, E., Schmid, B., Kretzschmar, H.A., Cruts, M., van Broeckhoven, C., Haass, C., Edbauer, D., 2013. The C9orf72 GGGGCC repeat is translated into aggregating dipeptide-repeat proteins in FTLD/ALS. Science (New York, N.Y.) 339 (6125), 1335–1338. https://doi.org/10.1126/SCIENCE.1232927.

Müller, G., Lübow, C., Weindl, G., 2020. Lysosomotropic beta blockers induce oxidative stress and IL23A production in Langerhans cells. Autophagy 16 (8), 1380. https://doi.org/10.1080/15548627.2019.1686728.

Nguyen, D.K.H., Thombre, R., Wang, J., 2019. Autophagy as a common pathway in amyotrophic lateral sclerosis. Neurosci. Lett. 697, 34–48. https://doi.org/10.1016/j.neulet.2018.04.006.

Nishida, Y., Arakawa, S., Fujitani, K., Yamaguchi, H., Mizuta, T., Kanaseki, T., Komatsu, M., Otsu, K., Tsujimoto, Y., Shimizu, S., 2009. Discovery of Atg5/Atg7-independent alternative macroautophagy. Nature 461 (7264), 654–658. https://doi.org/10.1038/NATURE08455.

Perera, N.D., Sheean, R.K., Lau, C.L., Shin, Y.S., Beart, P.M., Horne, M.K., Turner, B.J., 2018. Rilmenidine promotes MTOR-independent autophagy in the mutant SOD1 mouse model of amyotrophic lateral sclerosis without slowing disease progression. Autophagy 14 (3), 534–551. https://doi.org/10.1080/15548627.2017.1385674.

Riederer, M.A., Soldati, T., Shapiro, A.D., Lin, J., Pfeffer, S.R., 1994. Lysosome biogenesis requires Rab9 function and receptor recycling from endosomes to the trans-Golgi network. J. Cell Biol. 125 (3), 573–582. https://doi.org/10.1083/JCB.125.3.573.

Ross, C.A., Poirier, M.A., 2004. Protein aggregation and neurodegenerative disease. Nat. Med. 10 (7), S10. https://doi.org/10.1038/NM1066.

Rudnick, N.D., Griffey, C.J., Guarnieri, P., Gerbino, V., Wang, X., Piersaint, J.A., Tapia, J. C., Rich, M.M., Maniatis, T., 2017. Distinct roles for motor neuron autophagy early and late in the SOD1G93A mouse model of ALS. Proc. Natl. Acad. Sci. U. S. A. 114 (39), E8294–E8303. https://doi.org/10.1073/PNAS.1704294114/SUPPL_FILE/PNAS.201704294SI.PDF.

Sareen D, O'Rourke JG, Meera P, Muhammad AK, Grant S, Simpkinson M, Bell S, Carmona S, Ornelas L, Sahabian A, Gendron T, Petrucelli L, Baughn M, Ravits J, Harms MB, Rigo F, Bennett CF, Otis TS, Svendsen CN, Baloh RH. Targeting RNA foci in iPSC-derived motor neurons from ALS patients with a C9ORF72 repeat expansion. Sci Transl Med. 2013 Oct 23;5(208):208ra149. doi: 10.1126/scitranslmed.3007529.

Saxena, S., Roselli, F., Singh, K., Leptien, K., Julien, J.P., Gros-Louis, F., Caroni, P., 2013. Neuroprotection through excitability and mTOR required in ALS motoneurons to delay disease and extend survival. Neuron 80 (1), 80–96. https://doi.org/10.1016/J.NEURON.2013.07.027.

Sellier, C., Campanari, M., Julie Corbier, C., Gaucherot, A., Kolb-Cheynel, I., Oulad-Abdelghani, M., Ruffenach, F., Page, A., Ciura, S., Kabashi, E., Charlet-Berguerand, N., 2016. Loss of C9 ORF 72 impairs autophagy and synergizes with polyQ Ataxin-2 to induce motor neuron dysfunction and cell death. EMBO J. 35 (12), 1276–1297. https://doi.org/10.15252/embj.201593350.

Shen, K., Choe, A., Sabatini, D.M., 2017. Intersubunit crosstalk in the rag GTPase heterodimer enables mTORC1 to respond rapidly to amino acid availability. Mol. Cell 68 (3), 552–565.e8. https://doi.org/10.1016/j.molcel.2017.09.026.

Shen, K., Rogala, K.B., Chou, H.T., Huang, R.K., Yu, Z., Sabatini, D.M., 2019. Cryo-EM structure of the human FLCN-FNIP2-rag-ragulator complex. Cell 179 (6), 1319–1329.e8. https://doi.org/10.1016/j.cell.2019.10.036.

Shi, Y, Lin, S, Staats, KA, Li, Y, Chang, WH, Hung, ST, Hendricks, E, Linares, GR, Wang, Y, Son, EY, Wen, X, Kisler, K, Wilkinson, B, Menendez, L, Sugawara, T, Woolwine, P, Huang, M, Cowan, MJ, Ge, B, Koutsodendris, N, Sandor, KP, Komberg, J, Vangoor, VR, Senthilkumar, K, Hennes, V, Seah, C, Nelson, AR, Cheng, TY, Lee, SJ, August, PR, Chen, JA, Wisniewski, N, Hanson-Smith, V, Belgard, TG, Zhang, A, Coba, M, Grunseich, C, Ward, ME, van den Berg, LH, Pasterkamp, RJ, Trotti, D, Zlokovic, BV, Ichida, JK, 2018 Mar. Haploinsufficiency leads to neurodegeneration in C9ORF72 ALS/FTD human induced motor neurons. Nat Med 24 (3), 313–325. https://doi.org/10.1038/nm.4490.

Sullivan, P.M., Zhou, X., Robins, A.M., Paushter, D.H., Kim, D., Smolka, M.B., Hu, F., 2016. The ALS/FTLD associated protein C9orf72 associates with SMCR8 and WDR41 to regulate the autophagy-lysosome pathway. Acta Neuropathologica Communications 4 (1), 51. https://doi.org/10.1186/S40478-016-0324-5.

Tran, H., Moazami, M.P., Yang, H., McKenna-Yasek, D., Douthwright, C.L., Pinto, C., Metterville, J., Shin, M., Sanil, N., Dooley, C., Puri, A., Weiss, A., Wightman, N., Gray-Edwards, H., Marosfoi, M., King, R.M., Kenderdine, T., Fabris, D., Bowser, R., et al., 2022. Suppression of mutant C9orf72 expression by a potent mixed backbone antisense oligonucleotide. Nat. Med. 28 (1), 117–124. https://doi.org/10.1038/s41591-021-01557-6.

Vest, R.T., Chou, C.C., Zhang, H., Haney, M.S., Li, L., Laqtom, N.N., Chang, B., Shuken, S., Nguyen, A., Yerra, L., Yang, A.C., Green, C., Tanga, M., Abu-Remaileh, M., Bassik, M.C., Frydman, J., Luo, J., Wyss-Coray, T., 2022. Small molecule C381 targets the lysosome to reduce inflammation and ameliorate disease in models of neurodegeneration. Proc. Natl. Acad. Sci. U. S. A. 119 (11) https://doi.org/10.1073/PNAS.2121609119/-/DCSUPPLEMENTAL.

Voß, H., Schlumbohm, S., Barwikowski, P., Wurlitzer, M., Dottermusch, M., Neumann, P., Schlüter, H., Neumann, J.E., Krisp, C., 2022. HarmonizR enables data harmonization across independent proteomic datasets with appropriate handling of missing values. Nat. Commun. 13 (1), 3523. https://doi.org/10.1038/s41467-022-31007-x.

Webster, C.P., Smith, E.F., Bauer, C.S., Moller, A., Hautbergue, G.M., Ferraiuolo, L., Myszczynska, M.A., Higginbottom, A., Walsh, M.J., Whitworth, A.J., Kaspar, B.K., Meyer, K., Shaw, P.J., Grierson, A.J., de Vos, K.J., 2016. The C9orf72 protein interacts with Rab1a and the ULK1 complex to regulate initiation of autophagy. EMBO J. 35 (15), 1656–1676. https://doi.org/10.15252/EMBJ.201694401.

Webster, C.P., Smith, E.F., Grierson, A.J., de Vos, K.J., 2018. C9orf72 plays a central role in Rab GTPase-dependent regulation of autophagy. Small GTPases 9 (5), 399–408. https://doi.org/10.1080/21541248.2016.1240495.

Xi, Z., Zinman, L., Moreno, D., Schymick, J., Liang, Y., Sato, C., Zheng, Y., Ghani, M., Dib, S., Keith, J., Robertson, J., Rogaeva, E., 2013. Hypermethylation of the CpG island near the G4C2 repeat in ALS with a C9orf72 expansion. Am. J. Hum. Genet. 92 (6), 981–989. https://doi.org/10.1016/J.AJHG.2013.04.017.

Zhang, X., Li, L., Chen, S., Yang, D., Wang, Y., Zhang, X., Wang, Z., Le, W., 2011. Rapamycin treatment augments motor neuron degeneration in SOD1(G93A) mouse model of amyotrophic lateral sclerosis. Autophagy 7 (4), 412–425. https://doi.org/10.4161/AUTO.7.4.14541.

Zhang, Y.J., Jansen-West, K., Xu, Y.F., Gendron, T.F., Bieniek, K.F., Lin, W.L., Sasaguri, H., Caulfield, T., Hubbard, J., Daughrity, L., Chew, J., Belzil, V.v., Prudencio, M., Stankowski, J.N., Castanedes-Casey, M., Whitelaw, E., Ash, P.E.A., DeTure, M., Rademakers, R., et al., 2014. Aggregation-prone c9FTD/ALS poly(GA) RAN-translated proteins cause neurotoxicity by inducing ER stress. Acta Neuropathol. 128 (4), 505–524. https://doi.org/10.1007/S00401-014-1336-5/FIGURES/5.

Zhou, Q., Lehmer, C., Michaelsen, M., Mori, K., Alterauge, D., Baumjohann, D., Schludi, M.H., Greiling, J., Farny, D., Flatley, A., Feederle, R., May, S., Schreiber, F., Arzberger, T., Kuhm, C., Klopstock, T., Hermann, A., Haass, C., Edbauer, D., 2017. Antibodies inhibit transmission and aggregation of C9orf72 poly- GA dipeptide repeat proteins. EMBO Mol. Med. 9 (5), 687–702. https://doi.org/10.15252/emmm.201607054.

Zhou, G., Pang, Z., Lu, Y., Ewald, J., Xia, J., 2022. OmicsNet 2.0: a web-based platform for multi-omics integration and network visual analytics. Nucleic Acids Res. 50 (W1), W527–W533. https://doi:10.1093/nar/gkac376.

Zhu, Q., Jiang, J., Gendron, T.F., McAlonis-Downes, M., Jiang, L., Taylor, A., Diaz Garcia, S., Ghosh Dastidar, S., Rodriguez, M.J., King, P., Zhang, Y., la Spada, A.R., Xu, H., Petrucelli, L., Ravits, J., da Cruz, S., Lagier-Tourenne, C., Cleveland, D.W., 2020. Reduced C9ORF72 function exacerbates gain of toxicity from ALS/FTD-causing repeat expansion in C9orf72. Nat. Neurosci. 23 (5), 615–624. https://doi.org/10.1038/s41593-020-0619-5.

Zu, T., Liu, Y., Bañez-Coronel, M., Reid, T., Pletnikova, O., Lewis, J., Miller, T.M., Harms, M.B., Falchook, A.E., Subramony, S.H., Ostrow, L.W., Rothstein, J.D., Troncoso, J.C., Ranum, L.P.W., 2013. RAN proteins and RNA foci from antisense transcripts in C9ORF72 ALS and frontotemporal dementia. Proc. Natl. Acad. Sci. U. S. A. 110 (51) https://doi.org/10.1073/PNAS.1315438110/-/DCSUPPLEMENTAL/PNAS.201315438SI.PDF.